coatings

MDPI

Article

Carbon-Phenolic Ablators Modified by Ceramic Nanofilms Deposited via Atomic Layer Deposition (ALD) Technique

Rita Bottacchiari [1,*], Laura Borgese [2], Laura Paglia [1], Giulia Pedrizzetti [1], Francesco Marra [1] and Giovanni Pulci [1]

[1] Department of Chemical Engineering Materials Environment, Sapienza University of Rome, Via Eudossiana 18, 00184 Rome, Italy; laura.paglia@uniroma1.it (L.P.); giulia.pedrizzetti@uniroma1.it (G.P.); francesco.marra@uniroma1.it (F.M.); giovanni.pulci@uniroma1.it (G.P.)

[2] Chemistry for Technologies Laboratory, Department of Mechanical and Industrial Engineering, University of Brescia & INSTM RU of Brescia, via Branze 38, 25123 Brescia, Italy; laura.borgese@unibs.it

* Correspondence: rita.bottacchiari@uniroma1.it

Abstract: Ablative materials are widely employed to protect space vehicles from the extreme thermal conditions experienced during their flight into a planetary atmosphere. Carbon-phenolic ablators are composed of a phenolic matrix and a fibrous carbon reinforcement. In the present study, the fibrous reinforcement has been modified through the deposition of thin protective layers of zirconium oxide and aluminum oxide, with the objective of reducing fiber recession and oxidation. The depositions were carried out via atomic layer deposition (ALD), a method that allows for the controlled deposition of uniform and conformal coatings on the carbon felt fibers. The depositions were subsequently evaluated through SEM-EDS analysis. Pristine and ALD-modified felts were impregnated with a phenolic resin matrix and the ablation performance of the composite materials was evaluated through oxyacetylene flame tests. The results demonstrated that, in comparison to uncoated ablators, the ALD-modified samples exhibited enhanced performance in terms of mass loss and surface recession: compared to uncoated ablators, the former was 14% lower and the latter was diminished by 50%. Moreover, the morphological characterization of the tested specimens revealed a significantly reduced degree of oxidation of the coated fibers which were directly exposed to the flame.

Keywords: ablative materials; atomic layer deposition; oxyacetylene flame tests

Citation: Bottacchiari, R.; Borgese, L.; Paglia, L.; Pedrizzetti, G.; Marra, F.; Pulci, G. Carbon-Phenolic Ablators Modified by Ceramic Nanofilms Deposited via Atomic Layer Deposition (ALD) Technique. *Coatings* **2024**, *14*, 1551. https://doi.org/10.3390/coatings14121551

Academic Editors: José Guadalupe Quiñones-Galván and Laura Patricia Rivera Reséndiz

Received: 20 November 2024
Revised: 7 December 2024
Accepted: 9 December 2024
Published: 11 December 2024

1. Introduction

Ablative Thermal Protection Systems (A-TPS) are employed to protect spacecrafts undergoing atmospheric ballistic re-entry from the extreme thermal loads that they encounter. Low-density carbon-phenolic ablators are one of the most adopted heat shield families for the aforementioned missions. NASA-designed PICAs (Phenolic Impregnated Carbon Ablators) represent a notable example of this class of ablators [1]; they have been successfully employed for the protection of numerous capsules, including the Stardust Sample Return Capsule and the Crew Dragon [2,3]. PICAs consist of a phenolic resin matrix reinforced with a carbon fiber felt. The efficacy of such thermal shields is attributed to a combination of physical and chemical mechanisms, resumed under the term *ablation* and schematically depicted in Figure 1. During re-entry, part of the intense heat flux transfers inside the material, gradually increasing its temperature, and pyrolysis reactions begin to take place [4]. Pyrolysis is an endothermic reaction that results in the consumption of a significant amount of heat through the decomposition of the phenolic resin, which progresses from the exposed surface inwards [5]. Three layers can then be distinguished along with the thickness of the shield: the virgin material, the pyrolysis zone, and the charred material. The pyrolysis reactions generate two main products: pyrolysis gases and a solid carbonaceous residue. The outer residual material, known as *char*, is composed of carbonized resin and carbon fibers; it is highly porous, thus acting as an insulating

layer, and it re-radiates part of the incident heat from the surface [6–9]. Concurrently, the pyrolysis gases percolate through the char and out the material, carrying away additional heat, and exhaust into the boundary layer, further reducing the convective heat exchange through the *blockage effect* [10]. In addition to these beneficial effects, a number of undesired phenomena also participate in the ablation process, leading to the progressive removal of the char: the material is subjected to high shear stresses, extreme thermal load, high internal pressure due to pyrolysis gases and chemical reactions, including sublimation, nitridation, and oxidation [4,11]. The carbon fibers and the solid carbon residue react with the surrounding gases, which include oxygen in some planets' atmospheres like Earth's. When it takes place, oxidation weakens and partially consumes the surface char and fibers, leading to the easy removal of matter (surface recession) [7,12–14]. The fibrous reinforcement plays a significant role in the mechanical resistance of the char layer and is fundamental for the limitation of surface recession; therefore, enhancing its thermal and oxidation resistance can effectively enhance the overall efficiency of the ablator [15]. Much research has therefore been focused on modifying carbon fibers. Several authors [16–18] employed inert materials like alumina, titania, or zirconia to coat carbon fibers with the objective of improving their oxidation resistance by adding a layer of low oxygen permeability. Pan et al. [19] coated the carbon fibers of a carbon-phenolic ablator with nano-TiO_2 by sol–gel and calcination methods, obtaining ablators with improved oxidation resistance and IR radiation shielding properties, together with a reduction in surface recession. Xu et al. [20] deposited a silica sol/natural rubber coating on the carbon fiber felt prior to the impregnation with a phenolic aerogel matrix, thus preventing erosion from high-temperature oxidation and obtaining a composite with a lower mass loss rate and linear ablation rate in different high-temperature environments. Li et al. [21] coated the surface of carbon fibers of a C/C composite with HfB_2, thus decreasing the mass and linear ablation rates and enhancing the oxidation resistance of the fibers.

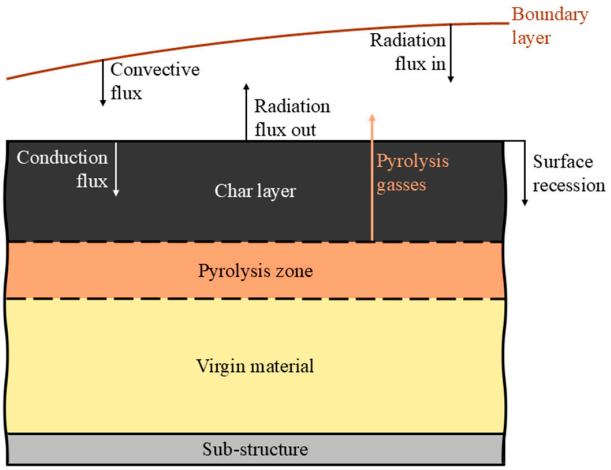

Figure 1. Scheme of the ablation process.

The deposition methods that are commonly used for inorganic oxides are the sol–gel method and Chemical Vapor Deposition (CVD). However, these techniques do not always result in the formation of a uniform coating, especially when coatings of low thickness are desired [17,22]. A good uniformity of the coating is necessary to effectively protect the fibers from oxidation and a low thickness is required to maintain unaffected the composite's characteristics, such as low weight and mechanical properties [22,23]. A technique by which a uniform and conformal thin coating can be deposited on a 3D substrate with complex shapes is atomic layer deposition (ALD) [24,25]. The uniformity and conformality of the coating can be achieved through ALD as it employs gaseous precursors which can diffuse inside the porosities of the material and then react with the surface sites of the substrate in multiple, controlled steps [18,26]. The formation of a uniform monoatomic

layer is promoted by overdosing the gaseous precursors which are introduced inside a reaction chamber, where they undergo sequential reactions on the substrate surface. The uniformity and purity of the coating is furthermore ensured by separating each reaction step by a purge step, during which the excess of gaseous precursors is evacuated. The desired coating thickness can be controlled by counting the number of reaction sequences and the conformity of the coating is enabled by the ability of the gas precursors to diffuse through the porosities of intricate and irregular geometries [18,27].

In the present work, carbon fiber felts were coated with nanometric films of Al_2O_3 and ZrO_2 by atomic layer deposition. ALD parameters were optimized to obtain a uniform coating of approximately 80 nm on the elevated specific surface area of the carbon. The coated and pristine felts were used as reinforcement in the production of carbon-phenolic ablators, achieved by impregnating the felts with a solution of phenolic resin and ethylene glycol. The introduction of the ceramic coatings, characterized by high melting points and thermal stability, is expected to reduce mass loss and surface recession of the ablators, without significantly altering the density of the virgin composite. The thermo-ablative performance of the ablators was evaluated using an oxyacetylene torch test: all samples were exposed to a 4 MW/m^2 heat flux and the surface and back temperatures were registered during the tests. The post-test analysis provided comparative data on mass loss and surface recession of the ablators, as well as insights into the different behavior of ceramic nanofilms.

2. Materials and Methods

2.1. Composite Raw Materials

A commercial rigid graphitic felt, Sigratherm MFA, was selected as reinforcement and purchased from SGL Carbon (SGL Carbon, Wiesbaden, Germany). It consists of randomly disposed carbon fibers connected by a carbon binder. SEM pictures of the fibrous material are reported in Figure 2.

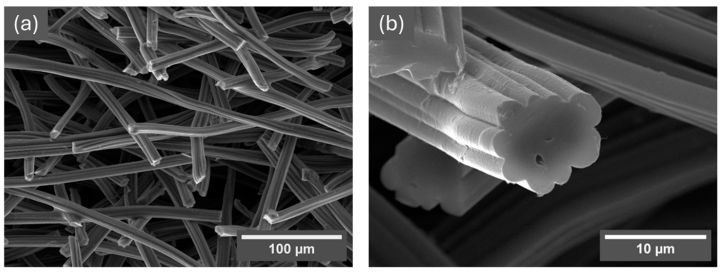

Figure 2. SEM images of the as-purchased carbon felt Sigratherm MFA. (**a**) low magnification image showing the fibers distribution; (**b**) higher magnification image showing a section of the carbon fibers.

A resol phenolic resin, Durite SC-1008 (Hexion Inc., Columbus, OH, USA), was selected as a matrix because of its high char yield and heat of ablation [9,28]. Ethylene glycol was selected as the solvent because its high boiling point (197 °C) allows a gel phase to form during the polymerization of the phenolic resin, which helps to ensure a homogeneous distribution of the resin inside the carbon felt [29].

2.2. Atomic Layer Deposition and Analysis

Tetrakis Dimethyl Amido Zirconium(IV) (TDMAZ) ($\geq$99.99% purity) and Trimethylaluminum (TMA) (97% purity) were used as zirconium and aluminum sources and purchased from Sigma-Aldrich (Merck KGaA, Darmstadt, Germany). Deionized (DI) water was used as an oxygen source and produced through the purification system Millipore DirectQ-5. Nitrogen (99.9999% purity) was purchased from Praxiar (Praxair Inc., Danbury CT, USA).

ZrO_2 and Al_2O_3 depositions were carried out using the Savannah 100 reactor system (Cambridge Nanotech Inc., Cambridge, MA, USA). Its cylindrical hot-wall reaction chamber can be heated to a fixed temperature, chosen according to the type of precursor and deposition process. A rotary pump was used to maintain the chamber pressure at $1.3{\cdot}10^{-5}$ MPa and to remove unreacted gasses and by-products.

Deposition parameters, such as pulse, exposure, and purging time were optimized for both ZrO_2 and Al_2O_3, while the deposition temperatures were chosen according to literature data [18,23,30]: zirconia was deposited with a chamber temperature of 250 °C and alumina was deposited at 200 °C. Pulse and exposure time were adjusted to ensure saturation of the elevated specific surface area of the Sigratherm MFA felt, estimated by the Brunauer–Emmett–Teller (BET (Micromeritics Instrument Corporation, Norcross, GA, USA) analysis to be 0.7 m^2/g. Similarly, purge time was chosen to guarantee the complete evacuation of by-products and unreacted species. N_2 flowed at 20 standard cubic centimeters per minute (sccm) during each step. A witness Si wafer was placed in the deposition chamber to monitor the deposition thickness by means of an experimental scale correlating the Si surface color with the thickness of the deposited layer; cycles were interrupted when a thickness of about 80 nm was obtained. The as-defined deposition parameters of zirconia and alumina films are summarized in Tables 1 and 2, respectively. A single ZrO_2 ALD cycle consists of the following: (i) pulse of the metal precursor for 5 s and an exposure time of 1 s; (ii) purge of the by-products and unreacted species with nitrogen gas for 80 s; (iii) pulse of DI water for 0.3 sec and an exposure time of 1 s; and (iv) purge with nitrogen gas for 80 s. The formation of the ZrO_2 layers can be described by the following reactions (Equations (1) and (2)) [30]:

$$||\text{–OH} + Zr(N(CH_3)_2)_{4\,(g)} \rightarrow ||\text{–O–}Zr(N(CH_3)_2)_3 + C_2H_7N_{(g)} \quad (1)$$

$$||\text{–O–}Zr(N(CH_3)_2)_3 + 3H_2O_{(g)} \rightarrow ||\text{–O–}Zr(OH)_3 + 3C_2H_7N_{\,(g)} \quad (2)$$

where || denotes the substrate surface. A total of 360 cycles were completed. The Al_2O_3 deposition cycle consists of the following: (i) pulse of the metal precursor for 0.3 s and an exposure time of 3 s; (ii) purge of the by-products and unreacted species with nitrogen gas for 80 s; (iii) pulse of DI water for 0.7 s and an exposure time of 3 s; and (iv) purge with nitrogen gas for 90 s. The formation of Al_2O_3 can be described by the following reactions (Equations (3) and (4)) [31]:

$$||\text{–OH} + Al(CH_3)_{3\,(g)} \rightarrow ||\text{–O–}Al(CH_3)_2 + CH_{4(g)} \quad (3)$$

$$||\text{–O–}Al(CH_3)_2 + 2H_2O_{(g)} \rightarrow ||\text{–O–}Al(OH)_2 + 2CH_{4(g)} \quad (4)$$

where || denotes the substrate surface. A total of 550 cycles were completed.

Table 1. Deposition parameters for ZrO_2.

Precursor	Chamber Temperature (°C)	Pulse (s)	Exposure (s)	Purge (s)	Cycles (#)
TDMAZ	250	5	1	80	360
Deionized H_2O	250	0.3	1	80	

Table 2. Deposition parameters for Al_2O_3.

Precursor	Chamber Temperature (°C)	Pulse (s)	Exposure (s)	Purge (s)	Cycles (#)
TMA	200	0.3	3	80	550
Deionized H_2O	200	0.7	3	90	

Carbon substrates can be functionalized before the deposition cycles to ensure the presence of -OH reaction sites adsorbed on the carbon surface, thus facilitating the nucleation of the ALD layers [18,32]. Therefore, the samples were exposed to DI H_2O for 10 cycles with the same parameters used for the depositions prior to the deposition cycles.

The characterization of the coated carbon felts was performed using a Tescan Mira 3 Scanning Electron Microscope (SEM) (Tescan, Brno, Czech Republic) equipped with an

Edax Octane Elect Energy Dispersive X-Ray Spectroscopy (EDS) system (Edax/Ametek Inc., Berwyn, PA, USA). Edax Team v.5 software was used for elementary analysis.

2.3. Manufacturing of the Composite

Both coated and uncoated carbon felts were impregnated with a solution of phenolic resin and ethylene glycol by adopting the same manufacturing procedure. The ratio of phenolic resin to ethylene glycol was chosen to obtain the desired final density (0.38 ± 0.01 g/cm^3) using the parameter *yield of curing cycle*, defined as the ratio between the mass of the cured resin (expressed in g) and the initial volume of the solution (expressed in ml), as described in a previous work [33]. The solution was heated on a magnetic stirring plate and maintained at 150 °C until the incipient formation of a gel phase was observed, indicating an advanced cross-linking of the resin. The mixture was then cooled to 60 °C and sonicated for 2 hours using a 505 Sonic Dismembrator sonic probe (Fisher Scientific, Hampton, NH, USA). The carbon felts were then fully immersed in the solution, which was reheated to 150 °C and stirred until complete gelation. Excess gel was removed from around the specimens and the final curing step was performed exposing the samples at 180 °C for 24 h in a furnace. The as-prepared samples will be referred to as: (i) Abl-Std, for the unmodified MFA impregnated with phenolic resin, taken as a reference; (ii) Abl-Zr, for the MFA modified by ALD zirconia film and impregnated with phenolic resin; and (iii) Abl-Al, for the alumina-modified MFA carbon felt impregnated with phenolic resin.

2.4. Oxyacetylene Torch Test

The oxyacetylene flame exposure test was adopted to assess the thermal insulation effectiveness, recession rate, and mass loss of the composite ablators when exposed to a heat flux consistent to the re-entry mission conditions. The tested specimens were of cylindrical shape and approximately 30 mm in height and 15 mm in diameter. The tests were carried out in accordance with the ASTM standard E 285–08 [34] using an apparatus schematized in Figure 3. A neutral flame was obtained by adjusting the oxygen/fuel ratio, as described elsewhere [28,29,35,36]: the flow rate was set at 315 NL/h for acetylene and 300 NL/h for oxygen; input parameters were managed using a virtual LabView environment (National Instruments, Austin, TX, USA) specifically developed for this application. All samples were tested for 60 s at a cold-wall heat flux value of 4 MW/m^2. The incident heat flux was set by adjusting the distance between the torch tip and the sample; an HFM 1000 heat flux sensor (Vatell Corporation, Christiansburg, VA, USA) was used to calibrate such distance prior to testing. The surface and the back temperatures of each sample were measured using an ISQ5-LO two-color digital pyrometer (LumaSense Technologies GmbH, Raunheim, Germany) and a K-type thermocouple placed inside the specimen at 20 mm from the exposed surface. Measurements were recorded by a cDAQ data-acquisition system (National Instruments, Austin, TX, USA). To quantify weight loss and surface recession, the dimensions and weight of each sample were measured before and after the test.

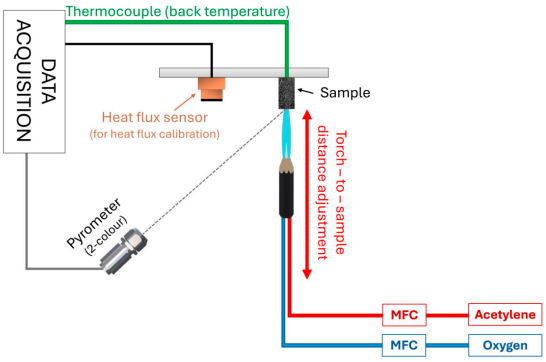

Figure 3. Oxyacetylene flame exposure test system.

3. Results and Discussion

3.1. Microstructural Characterization of the ALD Depositions

A cross-section of the samples was observed, and representative backscattered electron (BSE) micrographs are reported in Figure 4: pictures a-c show ZrO_2-coated carbon fibers at increasing magnifications; similarly, pictures d-f show the carbon felts coated with Al_2O_3. Low-magnification images show that the carbon fibers are largely uniformly coated. The high conformality of the coating can be observed in the high magnification images: the shape of the fiber is faithfully traced by the coating.

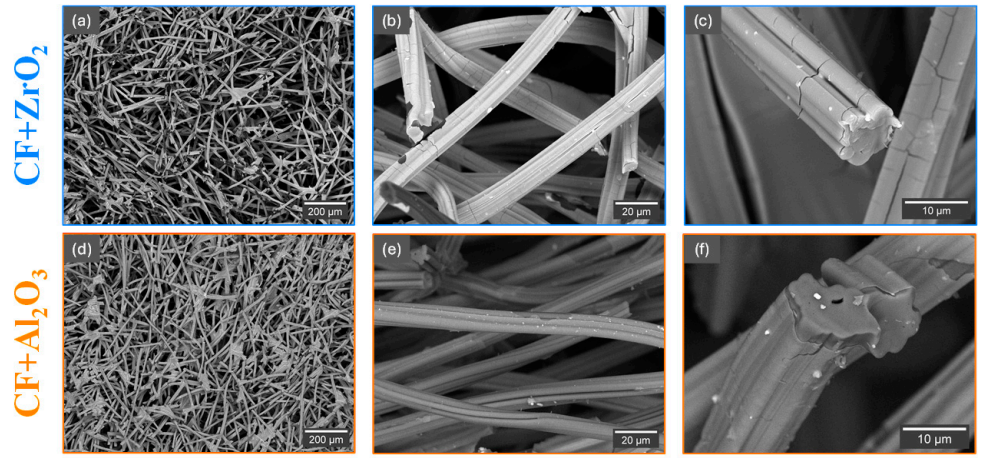

Figure 4. BSE cross-section micrographs of the carbon fibers (CF) coated with (**a**–**c**) zirconia and (**d**–**f**) alumina.

The cross-section micrographs show a partial delamination of the thin films, probably induced by the cutting procedure. The ALD film thickness was measured by performing image analyses on secondary electron (SE) micrographs, as shown in Figure 5b,d. The thickness of the zirconia layer (Figure 5a,b) is 87 ± 14 nm, while the alumina layer (Figure 4c,d) is 76 ± 17 nm thick.

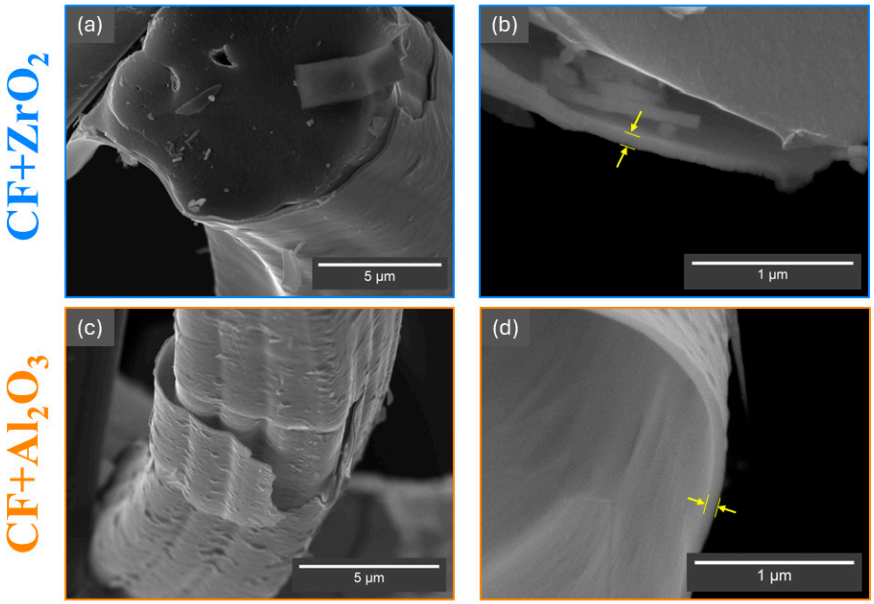

Figure 5. SE micrographs showing the thickness of the (**a**,**b**) zirconia and (**c**,**d**) alumina coatings.

The coatings composition was confirmed by the EDS analysis reported in Figure 6, in which, along with the C peak derived from the carbon fibers, the peaks of the Zr and O can

be identified in Figure 6b for the zirconia coating and Al and O peaks can be identified in Figure 6d for the alumina coating.

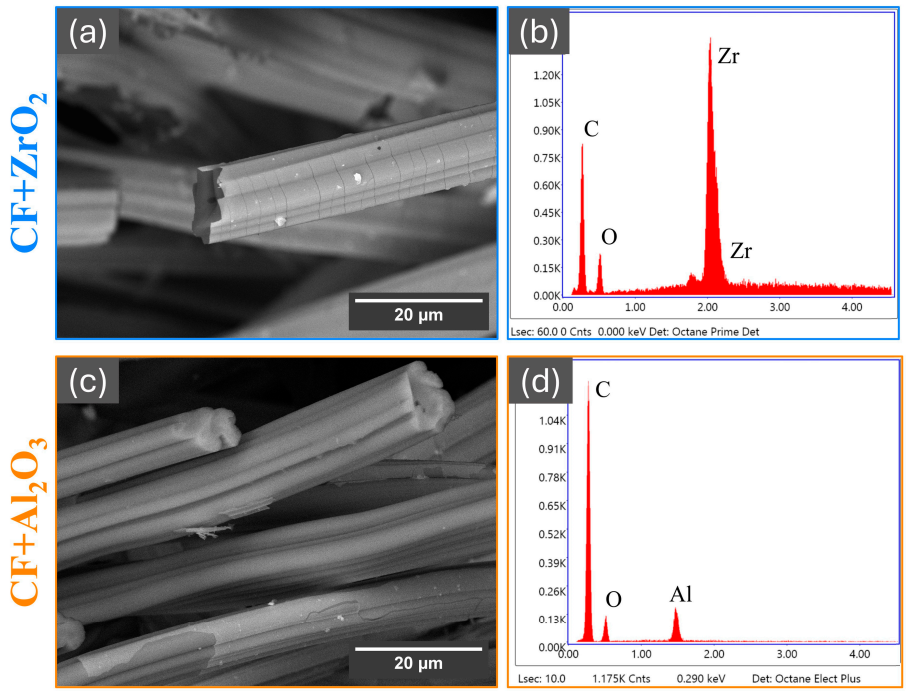

Figure 6. EDS analysis of the coated carbon fibers: (**a**) BSE images of the zirconia-coated fibers and related (**b**) EDS analysis; (**c**) BSE images of the alumina-coated fibers and related (**d**) EDS analysis.

3.2. Oxyacetylene Torch Test Results

Ablation tests were carried out exposing the samples to a heat flux of 4 MW/m^2 for 60 s. Ablation properties were evaluated by recording the surface and back temperatures during the oxyacetylene flame exposure and measuring variations in weight and height of each specimen before and after the tests. Test data obtained from the oxyacetylene flame exposure are reported in Table 3.

Table 3. Data of the oxyacetylene exposure tests.

Sample	Surface Temperature (°C)	Back Temperature (°C)	Recession (mm)	Mass Loss (%)
Abl-Std	2156 ± 55	754 ± 51	2.46 ± 0.70	44 ± 1
Abl-Zr	2178 ± 57	687 ± 47	1.22 ± 0.32	37 ± 1
Abl-Al	2156 ± 49	749 ± 50	1.24 ± 0.48	39 ± 1

The representative curves of temperature trends recorded during the oxyacetylene tests are presented in Figure 7. The temperature evolution of the exposed surface is similar for all samples. The Abl-Zr samples exhibit average back temperatures at the end of the tests that are slightly lower than Abl-Std; however, this reduction in temperature, which is approximately 65 °C, is accompanied by a standard deviation of approximately 50 °C. Therefore, from a statistical point of view, no significant changes in temperature evolution have been observed due to the presence of the ceramic coatings.

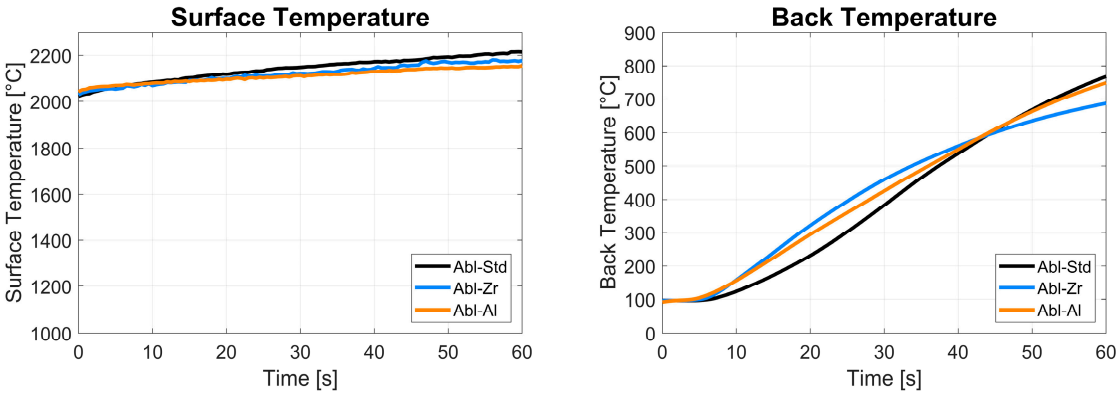

Figure 7. Trends of the surface and back temperatures measured during the oxyacetylene test.

Figure 8 shows the bar charts for mass loss and recession values. A comparable recession was observed for the ALD-modified ablators, 1.22 ± 0.32 mm for the Abl-Zr samples and 1.24 ± 0.48 mm for the Abl-Al samples, which is approximately 50% lower than that observed for the Abl-Std, whose recession was of 2.46 ± 0.70 mm. On the other hand, the mass loss of ALD-modified ablators, which has been normalized to the initial weight of the samples to compensate for any initial discrepancies, is only slightly lower than Abl-Std. In fact, mass loss can be attributed to both the pyrolysis of the phenolic resin [37] and the loss of the char layer consequent to surface recession. The pyrolysis of the phenolic resin occurs along the thickness of the material; the resin is distributed between the fibers and is first invested by the ablation phenomena [38]; therefore, no differences in the pyrolysis extent are expected to arise when the fibers are coated and the contribution of pyrolysis to the mass loss values is expected to be similar for all the tested samples. In contrast, recession is a surface phenomenon and occurs after the formation of the superficial char layer. Firstly, the phenolic resin pyrolyzes and a carbonous residue remains on the fibers; the char is then partially removed due to the mechanical stresses and oxidation phenomena [20,37,39]. Therefore, major differences introduced by the presence of the ceramic coatings are expected to be found in the degree of recession and only to a lower extent in the mass loss values.

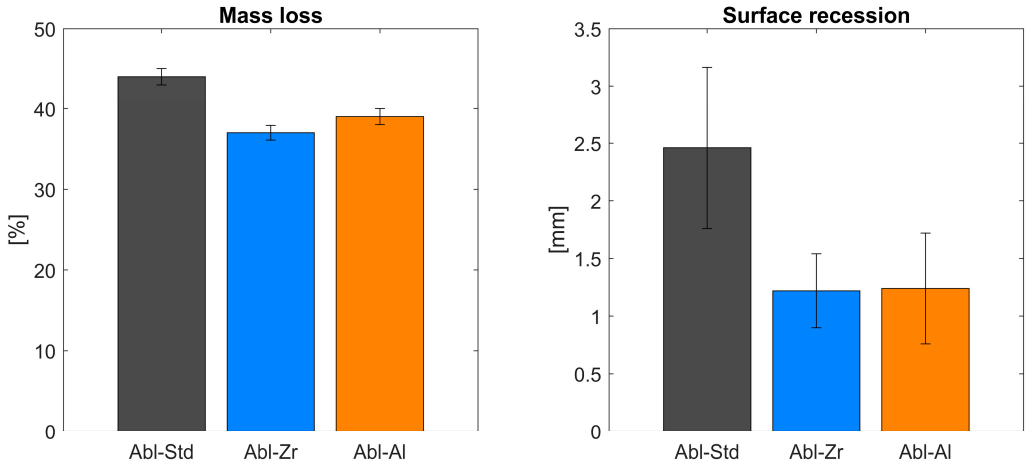

Figure 8. Bar charts for mass loss and recession measured during the oxyacetylene flame tests.

The pictures in Figure 6a,d,g show a cross-section view of the surface of the specimens after the tests, evidencing their different final geometries: the larger recession of Abl-Std is characterized by an irregular shape of the exposed surface, whereas the modified ablators preserved a more regular geometry, thus indicating the effectiveness of the coatings in protecting the fibers. To further investigate this phenomenon, higher magnification micrographs of the exposed surface of each representative sample were then examined and reported in Figure 9.

Abl-Std displays a notable consumption of the fibers, exhibiting pitting and icicle-shaped fibers indicative of massive oxidation phenomena (Figure 9c) [39–41] while ALD-modified samples show a lower amount of fiber consumption and oxidation (Figure 9f,i). Furthermore, given the Abl-Std has a much higher surface recession, the large fiber consumption is observed at a greater distance from the exposed surface if compared with the modified ablators. In Abl-Al and Abl-Zr, fibers are covered by the ALD oxide layers, which were able to reduce the oxidation phenomena and hamper fiber consumption. Figure 9f,i also illustrate the different behavior of the zirconia and alumina coatings as a consequence of flame exposure: zirconia forms a protective skeleton over the fibers well detectable after the exposure tests; conversely, only spherical particles of alumina can be observed on the Abl-Al fibers. This can be explained by considering that SEM micrographs in Figure 9 are acquired near the central zone of the specimens and that the melting point of alumina is slightly higher than 2000 °C. The registered surface temperatures of the samples demonstrate that this temperature was exceeded in the central zone, which was impinged by the core of the flame. It can therefore be assumed that the spherical particles are the result of the melting and subsequent re-solidification of the alumina layers. Micrographs at higher magnification of the Abl-Al sample surface close to the stagnation point are reported in Figure 10a,b. Figure 10c,d show the peripherical region of the exposed surface of Abl-Al in which the fibers are coated with an alumina skeleton, indicating that the maximum temperatures reached on the peripherical regions were not sufficient to reach the complete melting of the alumina films. Such behavior was not observed in the Abl-Zr, which exhibited a more homogeneous residual fiber coating because of the higher melting point of zirconia (>2700 °C), well above the maximum test temperature experienced by the samples. Representative images of the zirconia-coated fibers on the exposed surfaces are reported in Figure 10e,f.

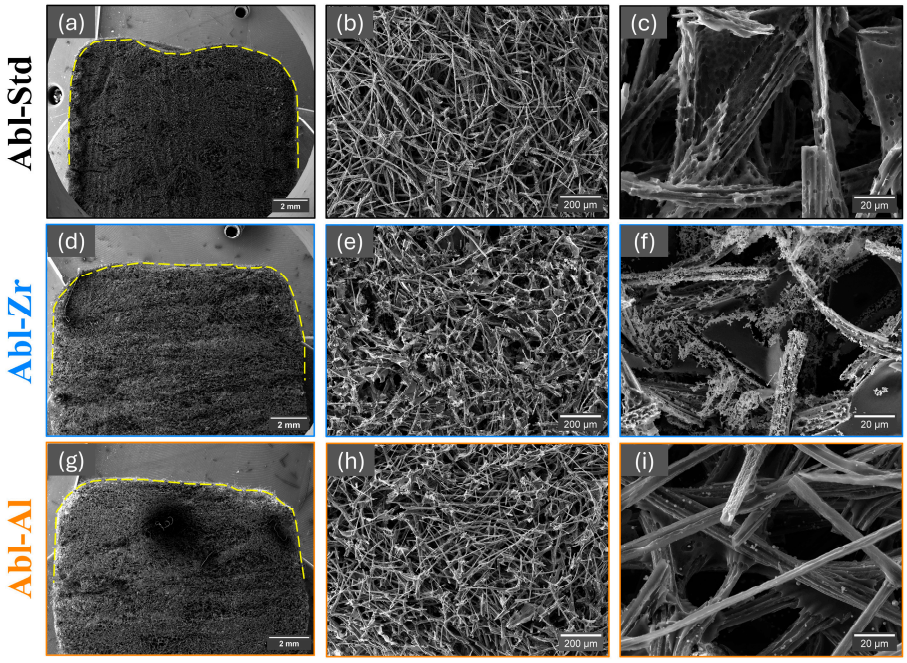

Figure 9. Cross-section (first column) and top-view (second and third column) micrographs of the exposed surfaces of (**a**–**c**) Abl-Std, (**d**–**f**) Abl-Zr, and (**g**–**i**) Abl-Al after the oxyacetylene flame test.

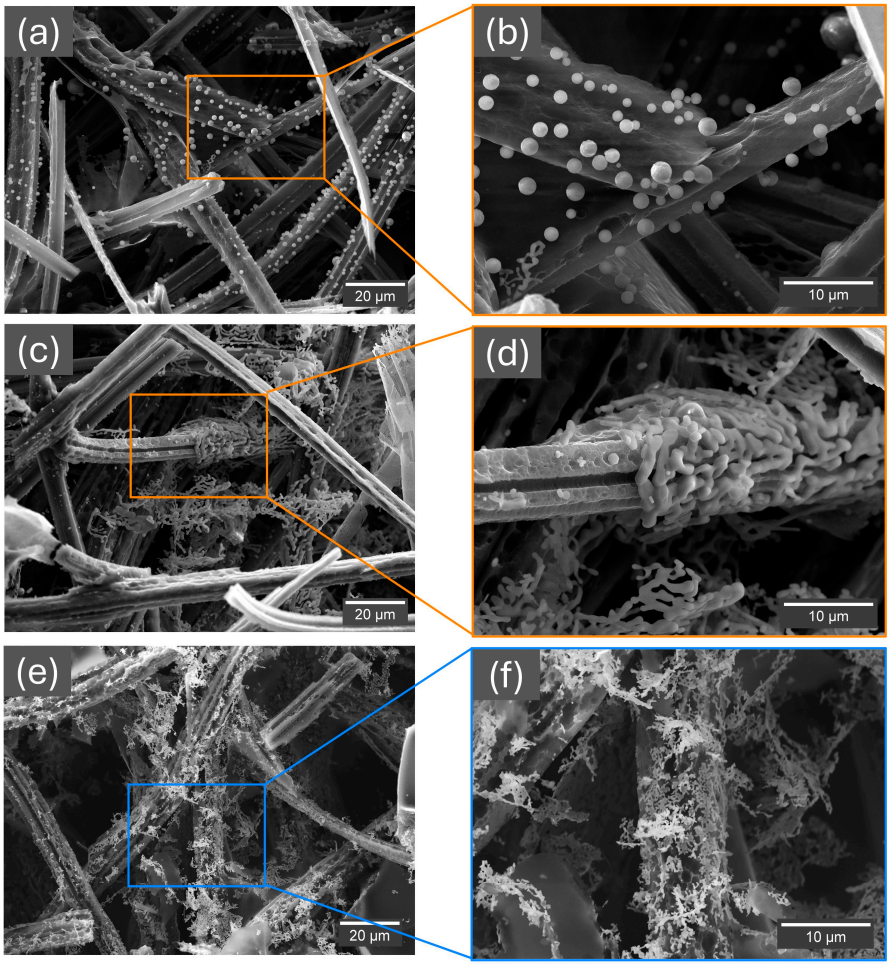

Figure 10. Images of (**a**–**d**) Abl-Al of the exposed surface after the oxyacetylene torch test taken in the central (**a**,**b**) and peripherical (**c**,**d**) regions; (**e**,**f**) Abl-Zr of the exposed surface after the oxyacetylene torch test.

4. Conclusions

A variety of carbon-phenolic ablative materials were produced using a carbon fiber felt reinforcement, which was modified through the incorporation of a thin ceramic film via atomic layer deposition. Much research is present in the literature on the protection of carbon fiber felts through a protective thin coating, but few works investigate their properties when the felts are employed in carbon-phenolic ablative. In this work, two oxides were deposited by the atomic layer deposition technique on the carbon fibers: alumina and zirconia. In order to evaluate the impact of the ceramic layers on the ablation performances, pristine carbon felts were employed as references. Each reinforcement was impregnated with a solution of phenolic resin and ethylene glycol, the ratio of which was selected to obtain a final composite density of approximately 0.38 g/cm^3.

The results of the ALD depositions were evaluated through SEM analysis, which revealed that the oxide layers are conformal to the irregular shape of the fibers, which are mostly uniformly covered. The deposited thicknesses were subsequently measured using scanning electron micrographs. Ablation properties were evaluated through oxyacetylene exposure tests and no significant differences among the three different ablators were measured in surface and back temperatures. Both modified ablators showed only a slight reduction in mass loss, which is primarily attributed to the ablation of the matrix and corresponds to a 14% diminishing compared to the standards. A consistent improvement in surface recession was observed for both Abl-Zr and Abl-Al samples, for which the recession was 50% lower than that of the Abl-Std. It is noteworthy that the recession was not only

lower in its overall value, but it was also much more homogeneous, thus indicating the efficacy of the coating in protecting the fibers from oxidation and consumption. Indeed, the SEM analysis of the tested samples shows that the fibers of the ALD-modified ablators are significantly less consumed and oxidized than the uncoated fibers.

The deposition of a thin oxide layer on the carbon fibers reinforcement has thus been demonstrated to enhance the ablation properties of the carbon-phenolic composites, particularly in terms of surface recession and, to a lesser extent, in mass loss. In addition to these benefits, the employed deposition technique allowed for the formation of nanometric films, thus maintaining unaltered felt porosities and having negligible consequences on the felt's weight.

Author Contributions: Conceptualization, G.P. (Giovanni Pulci), F.M., and L.P.; methodology, L.P. and L.B.; validation, L.P., R.B., G.P. (Giovanni Pulci), and F.M.; formal analysis, L.P. and R.B.; investigation, L.P., R.B., and L.B.; resources, G.P. (Giovanni Pulci); F.M. and L.B.; data curation, L.P., R.B., and G.P. (Giulia Pedrizzetti); writing—original draft preparation, R.B.; writing—review and editing, R.B., G.P. (Giovanni Pulci), L.P., and G.P. (Giulia Pedrizzetti); visualization, R.B. and L.P.; supervision, G.P. (Giovanni Pulci), F.M., and L.B.; project administration, G.P. (Giovanni Pulci), F.M., and L.B.; funding acquisition, G.P. (Giovanni Pulci), F.M., and L.B.; All authors have read and agreed to the published version of the manuscript.

Funding: This research received no external funding.

Data Availability Statement: The data presented in this study are available upon request from the corresponding author due to institutional policy.

Conflicts of Interest: The authors declare no conflicts of interest.

References

1. Bessire, B.K.; Lahankar, S.A.; Minton, T.K. Pyrolysis of Phenolic Impregnated Carbon Ablator (PICA). *ACS Appl. Mater. Interfaces* **2015**, *7*, 1383–1395. [CrossRef] [PubMed]
2. Stackpoole, M.; Sepka, S.; Cozmuta, I.; Kontinos, D. Post-Flight Evaluation of Stardust Sample Return Capsule Forebody Heatshield Material. In Proceedings of the 46th AIAA Aerospace Sciences Meeting and Exhibit, Reno, NV, USA, 7–10 January 2008; American Institute of Aeronautics and Astronautics: Reston, VA, USA, 2008. [CrossRef]
3. Nowlin, S.; Thimons, L. Surviving the heat: The application of phenolic impregnated carbon ablators. Available online: https://spacex.com.pl/files/2017-11/pica-x.pdf (accessed on 17 September 2024).
4. Lachaud, J.; Cozmuta, I.; Mansour, N.N. Multiscale Approach to Ablation Modeling of Phenolic Impregnated Carbon Ablators. *J. Spacecr. Rocket.* **2010**, *47*, 910–921. [CrossRef]
5. Bessire, B.K.; Minton, T.K. Decomposition of Phenolic Impregnated Carbon Ablator (PICA) as a Function of Temperature and Heating Rate. *ACS Appl. Mater. Interfaces* **2017**, *9*, 21422–21437. [CrossRef]
6. Srikanth, I.; Daniel, A.; Kumar, S.; Padmavathi, N.; Singh, V.; Ghosal, P.; Kumar, A.; Devi, G.R. Nano silica modified carbon–phenolic composites for enhanced ablation resistance. *Scr. Mater.* **2010**, *63*, 200–203. [CrossRef]
7. Grigat, F.; Loehle, S.; Zander, F.; Fasoulas, S. Spallation on Carbon Ablators. *AIAA J.* **2022**, *60*, 3936–3949. [CrossRef]
8. Mathieu, R.D. Mechanical spallation of charring ablators in hyperthermal environments. *AIAA J.* **1964**, *2*, 1621–1627. [CrossRef]
9. Cho, D.; Yoon, B.I. Microstructural interpretation of the effect of various matrices on the ablation properties of carbon-fiber-reinforced composites. *Compos. Sci. Technol.* **2001**, *61*, 271–280. [CrossRef]
10. Reynier, P. Survey of convective blockage for planetary entries. *Acta Astronaut.* **2013**, *83*, 175–195. [CrossRef]
11. Allcorn, E.K.; Natali, M.; Koo, J.H. Ablation performance and characterization of thermoplastic polyurethane elastomer nanocomposites. *Compos. Part A Appl. Sci. Manuf.* **2013**, *45*, 109–118. [CrossRef]
12. Panerai, F.; Mansour, N.N.; Lachaud, J.; Martin, A. Numerical and experimental study of carbon fiber oxidation. In Proceedings of the 52nd Aerospace Sciences Meeting, National Harbor, MD, USA, 13–17 January 2014; American Institute of Aeronautics and Astronautics: Reston, VA, USA, 2014. [CrossRef]
13. Zuo, H.; Ruan, F.; Wang, H.; Wang, H.; Wang, X.; Huang, Y.; Wang, R.; Zou, L.; Xu, Z.; Li, D. Advances in Ablation or Oxidation Mechanisms and Behaviors of Carbon Fiber-Reinforced Si-Based Composites. *Molecules* **2023**, *28*, 6022. [CrossRef]
14. Panerai, F.; Cochell, T.; Martin, A.; White, J.D. Experimental measurements of the high-temperature oxidation of carbon fibers. *Int. J. Heat Mass Transf.* **2019**, *136*, 972–986. [CrossRef]
15. Ferguson, J.C.; Panerai, F.; Lachaud, J.; Mansour, N.N. Theoretical study on the micro-scale oxidation of resin-infused carbon ablators. *Carbon* **2017**, *121*, 552–562. [CrossRef]
16. Li, S.; Zhang, Y.; Zhou, Y. Preparation and characterization of sol–gel derived zirconia coated carbon fiber. *Surf. Coatings Technol.* **2012**, *206*, 4720–4724. [CrossRef]

17. Roy, A.K.; Schulze, S.; Hietschold, M.; Goedel, W.A. Oxidation protection of carbon fibers by coating with alumina and/or titania using atomic layer deposition. *Carbon* **2012**, *50*, 761–770. [CrossRef]
18. Widmer, J.T.; George, S.M. Al2O3 atomic layer deposition on a porous matrix of carbon fibers (FiberForm) for oxidation resistance. *J. Vac. Sci. Technol. A* **2023**, *41*, 062412. [CrossRef]
19. Pan, Y.; Jin, X.; Wang, H.; Huang, H.; Wu, C.; Yan, X.; Hong, C.; Zhang, X. Nano-TiO2 coated needle carbon fiber reinforced phenolic aerogel composite with low density, excellent heat-insulating and infrared radiation shielding performance. *J. Mater. Sci. Technol.* **2023**, *152*, 181–189. [CrossRef]
20. Xu, W.; Song, W.; Jia, X.; Ma, C.; Wang, J.; Qiao, W.; Ling, L. Nano-silica modified lightweight and high-toughness carbon fiber/phenolic ablator with excellent thermal insulation and ablation performance. *Def. Technol.* **2023**, *31*, 192–199. [CrossRef]
21. Li, H.; Yao, D.; Fu, Q.; Liu, L.; Zhang, Y.; Yao, X.; Wang, Y.; Li, H. Anti-oxidation and ablation properties of carbon/carbon composites infiltrated by hafnium boride. *Carbon* **2013**, *52*, 418–426. [CrossRef]
22. Knohl, S.; Roy, A.K.; Goedel, W.A.; Schulze, S.; Hietschold, M. Atomic layer deposition onto carbon fiber: From single layer deposition via multilayer structure to metal oxide microtubes. *J. Vac. Sci. Technol. A Vac. Surf. Film.* **2013**, *31*, 01A139. [CrossRef]
23. Mohseni, H.; Scharf, T.W. Atomic layer deposition of ZnO/Al2O3/ZrO2 nanolaminates for improved thermal and wear resistance in carbon-carbon composites. *J. Vac. Sci. Technol. A Vac. Surf. Film.* **2012**, *30*, 01A149. [CrossRef]
24. Cremers, V.; Puurunen, R.L.; Dendooven, J. Conformality in atomic layer deposition: Current status overview of analysis and modelling. *Appl. Phys. Rev.* **2019**, *6*, 021302. [CrossRef]
25. Kemell, M.; Ritala, M.; Leskelä, M.; Groenen, R.; Lindfors, S. Coating of Highly Porous Fiber Matrices by Atomic Layer Deposition. *Chem. Vap. Depos.* **2008**, *14*, 347–352. [CrossRef]
26. Fang, W.-Z.; Tang, Y.-Q.; Ban, C.; Kang, Q.; Qiao, R.; Tao, W.-Q. Atomic layer deposition in porous electrodes: A pore-scale modeling study. *Chem. Eng. J.* **2019**, *378*, 122099. [CrossRef]
27. Maske, V.A.; More, A.P. Conformal coatings for lithium-ion batteries: A comprehensive review. *Prog. Org. Coatings* **2024**, *188*, 108252. [CrossRef]
28. Paglia, L.; Bottacchiari, R.; Cognigni, F.; Cerra, S.; Genova, V.; Rossi, M.; Fratoddi, I.; Marra, F.; Pulci, G. Micro and nanostructured carbon-phenolic ablators modified by PVP addition. *Mater. Des.* **2024**, *242*, 113014. [CrossRef]
29. Paglia, L.; Mapelli, C.; Genova, V.; Bracciale, M.P.; Marra, F.; Bartuli, C.; Fratoddi, I.; Pulci, G. Effect of ceramic nano-particles on the properties of a carbon-phenolic ablator. *Polym. Compos.* **2022**, *43*, 7345–7359. [CrossRef]
30. Liu, J.; Meng, X.; Hu, Y.; Geng, D.; Banis, M.N.; Cai, M.; Li, R.; Sun, X. Controlled synthesis of Zirconium Oxide on graphene nanosheets by atomic layer deposition and its growth mechanism. *Carbon* **2013**, *52*, 74–82. [CrossRef]
31. Ott, A.; Klaus, J.; Johnson, J.; George, S. Al3O3 thin film growth on Si(100) using binary reaction sequence chemistry. *Thin Solid Films* **1997**, *292*, 135–144. [CrossRef]
32. Roy, A.K.; Baumann, W.; Schulze, S.; Hietschold, M.; Mäder, T.; Nestler, D.J.; Wielage, B.; Goedel, W.A. Atomic Layer Deposition of Alumina onto Carbon Fibers. *J. Am. Ceram. Soc.* **2011**, *94*, 2014–2022. [CrossRef]
33. Paglia, L.; Tirillò, J.; Marra, F.; Bartuli, C.; Simone, A.; Valente, T.; Pulci, G. Carbon-phenolic ablative materials for re-entry space vehicles: Plasma wind tunnel test and finite element modeling. *Mater. Des.* **2016**, *90*, 1170–1180. [CrossRef]
34. *ASTM International E285-08*; Standard Test Method for Oxyacetylene Ablation Testing of Thermal Insulation Materials. American Society for Testing and Materials: West Conshohocken, PA, USA, 2020.
35. Marra, F.; Pulci, G.; Tirilló, J.; Bartuli, C.; Valente, T. Numerical Simulation of Oxy-Acetylene Testing Procedure of Ablative Materials for Re-Entry Space Vehicles. *Proc. Inst. Mech. Eng. Part L J. Mater. Des. Appl.* **2011**, *225*, 32–40. [CrossRef]
36. Paglia, L.; Genova, V.; Bracciale, M.P.; Bartuli, C.; Marra, F.; Natali, M.; Pulci, G. Thermochemical characterization of polybenzimidazole with and without nano-ZrO2 for ablative materials application. *J. Therm. Anal. Calorim.* **2020**, *142*, 2149–2161. [CrossRef]
37. Wong, H.-W.; Peck, J.; Assif, J.; Panerai, F.; Lachaud, J.; Mansour, N.N. Detailed analysis of species production from the pyrolysis of the Phenolic Impregnated Carbon Ablator. *J. Anal. Appl. Pyrolysis* **2016**, *122*, 258–267. [CrossRef]
38. Sessim, M.; Shi, L.; Calvert, T.J.; Phillpot, S.R.; Tonks, M.R. Phase-field model of char oxidation in ablative thermal protection system materials. *Comput. Mater. Sci.* **2024**, *233*, 112713. [CrossRef]
39. Helber, B.; Turchi, A.; Scoggins, J.B.; Hubin, A.; Magin, T.E. Experimental investigation of ablation and pyrolysis processes of carbon-phenolic ablators in atmospheric entry plasmas. *Int. J. Heat Mass Transf.* **2016**, *100*, 810–824. [CrossRef]
40. Panerai, F.; Martin, A.; Mansour, N.N.; Sepka, S.A.; Lachaud, J. Flow-Tube Oxidation Experiments on the Carbon Preform of a Phenolic-Impregnated Carbon Ablator. *J. Thermophys. Heat Transf.* **2014**, *28*, 181–190. [CrossRef]
41. Helber, B.; Chazot, O.; Hubin, A.; Magin, T.E. Microstructure and gas-surface interaction studies of a low-density carbon-bonded carbon fiber composite in atmospheric entry plasmas. *Compos. Part A Appl. Sci. Manuf.* **2015**, *72*, 96–107. [CrossRef]